

## Simulation of nanocolumn formation in a plasma environment

J. W. Abraham, N. Kongsuwan, T. Strunskus, F. Faupel, and M. Bonitz

Citation: *Journal of Applied Physics* **117**, 014305 (2015); doi: 10.1063/1.4905255

View online: <http://dx.doi.org/10.1063/1.4905255>

View Table of Contents: <http://scitation.aip.org/content/aip/journal/jap/117/1?ver=pdfcov>

Published by the AIP Publishing

---

### Articles you may be interested in

Magnetic field induced phase transformation in polycrystalline NiCoMnAl thin films

*Appl. Phys. Lett.* **103**, 132404 (2013); 10.1063/1.4821945

Formation of magnetic nanocolumns during vapor phase deposition of a metal-polymer nanocomposite:

Experiments and kinetic Monte Carlo simulations

*J. Appl. Phys.* **114**, 044305 (2013); 10.1063/1.4816252

Arrays of ordered nanostructures in Fe-Pt thin films by self-assembling of polystyrene nanospheres

*J. Appl. Phys.* **113**, 17B516 (2013); 10.1063/1.4797626

A quasicore-shell structure of FeCo and FeNi nanoparticles

*J. Appl. Phys.* **108**, 104314 (2010); 10.1063/1.3514089

Self-organization of ultrahigh-density Fe–Ni–Co nanocolumns in Teflon® AF

*Appl. Phys. Lett.* **88**, 123103 (2006); 10.1063/1.2187436

---



SUBSCRIBE TO  
**physics**  
**today**

# Simulation of nanocolumn formation in a plasma environment

J. W. Abraham,<sup>1</sup> N. Kongsuwan,<sup>1,2</sup> T. Strunkus,<sup>3</sup> F. Faupel,<sup>3</sup> and M. Bonitz<sup>1,a)</sup>

<sup>1</sup>Institut für Theoretische Physik und Astrophysik, Christian-Albrechts-Universität zu Kiel, Leibnizstraße 15, D-24098 Kiel, Germany

<sup>2</sup>Department of Physics, Cavendish Laboratory, J J Thomson Avenue, Cambridge CB3 0HE, United Kingdom

<sup>3</sup>Institut für Materialwissenschaft, Lehrstuhl für Materialverbunde, Christian-Albrechts-Universität zu Kiel, Kaiserstraße 2, D-24143 Kiel, Germany

(Received 23 October 2014; accepted 18 December 2014; published online 5 January 2015)

Recent experiments and kinetic Monte Carlo (KMC) simulations [H. Greve *et al.*, *Appl. Phys. Lett.* **88**, 123103 (2006), L. Rosenthal *et al.*, *J. Appl. Phys.* **114**, 044305 (2013)] demonstrated that physical vapor co-deposition of a metal alloy (Fe-Ni-Co) and a polymer (Teflon AF) is a suitable method to grow magnetic nanocolumns in a self-organized one-step process. While only thermal sources have been used so far, in this work, we analyze the feasibility of this process for the case of a sputtering source. For that purpose, we extend our previous simulation model by including a process that takes into account the influence of ions impinging on the substrate. The simulation results predict that metal nanocolumn formation should be possible. Furthermore, we show that the effect of ions that create trapping sites for the metal particles is to increase the number of nanocolumns.

© 2015 AIP Publishing LLC. [<http://dx.doi.org/10.1063/1.4905255>]

## I. INTRODUCTION

Modern technology is replete with nanoscale materials, which is owed to the ongoing success of the related research since the end of the 20th century. In contrast to classical materials, nanomaterials are characterized by a relatively high number of atoms or molecules on the surface in comparison to the bulk.<sup>1</sup> In recent years, nanocomposites have continuously attracted attention. The reason is the impressive variety of their functional applications, e.g., in electronics,<sup>2–5</sup> plasmonics,<sup>6,7</sup> food packaging,<sup>8</sup> and medicine.<sup>9,10</sup> In particular, metal-polymer nanocomposites consisting of metallic filler particles that are embedded in a polymer matrix offer numerous new applications.<sup>10–13</sup> Although self-organization plays a crucial role for the production of composites, experimentalists look for ways to have individual control over properties such as the particle size and the volume filling factor.

In a previous work, we reported on the experimental realization of the formation of Fe-Ni-Co nanocolumnar structures in a fluoropolymer matrix.<sup>14</sup> New experimental data as well as comprehensive computational studies for the same system were published recently.<sup>15</sup> The nanocomposite films of thicknesses ranging from 100 nm to 200 nm were produced by physical vapor co-deposition of metal and polymer. It could be shown in, both, experiments and simulations that the columns can only be produced if the metal deposition rate is much higher than that of the polymer. This was explained by the fact that columnar growth is only possible if the metallic clusters become so big that they undergo a phase transition from a liquid-like behavior with spherical growth to a solidified state with columnar growth. A comparison between a transmission electron microscopy (TEM)

image of experimental results and a rendered visualization of corresponding computer simulations is shown in Fig. 1.

As has been demonstrated in Ref. 15, one can successfully apply the kinetic Monte Carlo (KMC) method to describe the behavior of the system with a simplified but consistent model of all physical processes. Such an idealized description invokes basic geometric shapes that replace complicated atomic structures. The whole dynamics of the system are driven by diffusion, deposition, evaporation, and particle growth events.

In the aforementioned experiment, both the metallic components and the polymer were simultaneously deposited by thermal evaporation and subsequent condensation on the substrate. However, for some applications, it is useful to replace the sources of the deposited materials. In these cases, it is important to know if and how this will affect the resulting metallic structures. Therefore, in this work, we investigate the behavior of the nanocomposite formation for the situation of sputtered metal atoms in a complex plasma environment. Some recent overviews of the relevant experimental techniques, e.g., magnetron sputtering, are given in Refs. 10 and 16. A key property of the sputter deposition is

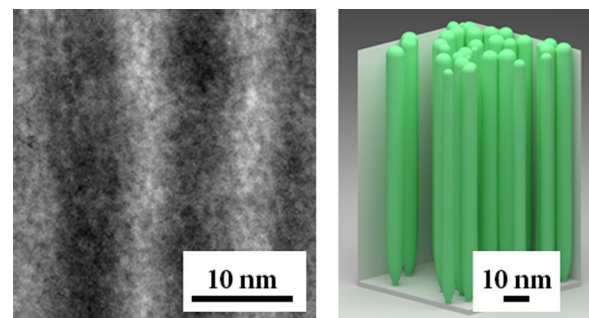


FIG. 1. Comparison between an TEM micrograph from the experiment (left) and a visualized simulation result (right).<sup>14,15</sup> In the TEM image, the columns appear dark.

<sup>a)</sup>bonitz@physik.uni-kiel.de

the occurrence of highly energetic ions that create defects in the polymer matrix.<sup>17</sup> In order to take this into account, we extended our simulation model by adding a process that randomly generates defect sites in the polymer matrix. These defects trap metal particles if they come sufficiently close. On the one hand, a defect may serve as a nucleation site for clusters that eventually might turn into a columnar structure. On the other hand, the defects effectively reduce the cluster diffusion, which is one of the driving forces of the column growth. In this paper, we show that the nanocolumn growth is even enhanced by this complex interplay, i.e., the additional defects that originate from the plasma environment lead to a highly increased number of columns with a reduced width.

A further extension of our previous model is an additional process that allows the metal particles to diffuse in the polymer bulk and not just on the surface. Scanning a large range of bulk diffusion constants, we observe that the influence of this process is relatively small for realistic parameter values, where the surface diffusion is much faster than the diffusion in the polymer matrix.

Although there exist accurate approaches to describe the impact of ions into matter,<sup>18</sup> the exact number of defects, their specific interactions with the bulk material and their geometries are not known in detail. The advantage of kinetic Monte Carlo is that it allows one to study comparatively large systems and to perform comprehensive parameter scans. Thus, even though we use a simple model that assumes spherical defects with extensions that are comparable to atoms, we expect to capture the main trends and realistic statistical behavior.

We start our presentation by recalling the basic ideas of the simulation model in Sec. II. Thereafter, in Sec. III, we separately discuss the influence of defects considering two cases: defects that are initially present on the substrate and defects that are randomly created during the whole deposition process.

## II. SIMULATION MODEL

We performed our simulations with the first-reaction algorithm, which is a widely used KMC method.<sup>19–22</sup> Especially for the particle-based simulation of nanocomposite formation, KMC simulations turned out to be a valuable tool since they allow for simplified but accurate self-consistent descriptions of highly complex systems of macroscopic size.<sup>21–24</sup> In order to handle the complicated dynamics of nanocomposites, some drastic, but at the same time carefully chosen approximations are employed. The main idea behind the simulations is to condense all relevant physical effects into the behavior of simple geometric bodies. The time dependence is driven by pre-defined rates for the execution of elementary processes. These rates are determined by the material properties as well as the system temperature. More details can be found, e.g., in Ref. 20. Given a process  $i$  with the rate  $\nu_i$ , the time  $t$  remaining until the execution of the process is always drawn from the exponential distribution

$$f(t) = \nu \exp(-\nu t). \quad (1)$$

All processes are executed according to the order of the randomly chosen process times. After each execution, the list of possible processes is updated.

In Subsections II A and II B we explain the employed model and go into the details of the spherical and the columnar growth.

### A. Elementary processes

The simulation model is based on the model in Ref. 15. The metal atoms are represented by spheres with the radius 0.145 nm. This value is chosen as it approximates the Wigner-Seitz radii of Iron, Nickel, and Cobalt, which are in between 0.144 nm and 0.147 nm. Using the Wigner-Seitz radius to define the atomic volume, we make sure that the density is conserved, when metal particles coalesce. As is typical of sputter deposition, we assume that only monomers impinge on the surface. The corresponding deposition rate is denoted by  $R_m$ . Metal clusters, which are formed by smaller clusters or monomers, are assumed to preserve a spherical shape. The treatment of the polymer matrix is restricted to the simple definition of a surface which, on the one hand, marks the height in  $z$ -direction of deposited monomers and, on the other hand, separates the diffusing surface clusters from nearly immobile clusters buried in the bulk. After each simulation step with the time difference  $\Delta t$ , the surface is raised by  $\Delta t \cdot R_p$ , where  $R_p$  is the pre-defined deposition rate of the polymer. In addition to this, each deposited metal atom shifts the surface by a small value that can be calculated with the density of a metallic monolayer (10 atoms/nm<sup>2</sup>). In the same way, the surface height is lowered whenever a metal atom evaporates. Hence, the time-dependence of the surface height can be rather complicated, because the amount of evaporated atoms strongly depends on the variable structure of the surface. While the deposition rate of metallic monomers is kept at the constant value  $R_m = 0.8$  nm/min, we only change the deposition rate of the polymer,  $R_p$ . This allows us to use the ratio  $\kappa = R_m/R_p$  to analyze the influence of the deposition rates on our results.

As long as they are not buried by the surface, all deposited monomers and newly formed clusters of size  $n$  may diffuse on the surface with the jump length 0.6 nm and the diffusion coefficient

$$D_s^n = n^{-1} D_s^1, \quad (2)$$

corresponding to the diffusion rate  $\nu_s^n = 4D_s^n/l^2$ . While surface diffusion is possible for clusters of all sizes, there is a finite probability that a monomer leaves the surface again. This process accounts for the characteristic experimental observation that a monomer performs a random walk on the surface before it is re-emitted.<sup>25</sup> We control this behavior via the evaporation rate  $R_e$ , which is given in units of the rate  $\nu_s^1$ .

A cluster is defined to be buried if the distance between the surface and the center of the cluster is greater than the radius of the cluster. For most of the results that are shown in this work, buried clusters are assumed to be trapped in the polymer. However, since diffusion in the polymer matrix is

known to be important under certain circumstances,<sup>23,26,27</sup> we performed additional calculations to investigate the influence of bulk diffusion. In accordance with the so-called free-volume theory,<sup>21,23,28</sup> the diffusion coefficient for bulk diffusion is approximated by

$$D_b^n = 2^{-n} D_b^1, \quad (3)$$

where we set

$$D_b^1 = \frac{D_s^1}{r_{s/b}}. \quad (4)$$

Hence, the free parameter  $r_{s/b}$  denotes the ratio between the surface and the bulk diffusion constants for monomers. The neglect of bulk diffusion corresponds to the limit  $r_{s/b} \rightarrow \infty$ . While surface diffusion is realized by jumps on a two-dimensional plane, the bulk diffusion is a movement in three-dimensional space. If bulk diffusion is allowed, not only the buried clusters may move in the bulk but also the clusters on the surface have the chance to move downwards into the bulk. This additional bulk diffusion process then competes with surface diffusion and re-emission.

As mentioned above, we extend the model of Ref. 15 by allowing the clusters to be trapped at defect sites in the polymer. These defects may either be intentionally produced on the substrate before the deposition or they may occur as a random process if the composite is produced in a sputtering process, where highly energetic ions impinge on the surface. In our simulations, we model a defect by a sphere with the radius  $r_{\text{defect}} = 0.3 \text{ nm}$ . Whenever a particle encounters such a defect, it is assumed to be trapped and keeps its current position. In this work, we will first show the influence of the number density of defects that are placed on the substrate initially. After that we cover the case of randomly created surface defects during the whole deposition process. This process is controlled via the ratio  $\gamma := R_{\text{defect}}/R_m$ , where  $R_{\text{defect}}$  is the rate for the creation of a single defect anywhere on the current surface during the ongoing simulation.

An illustration of all mentioned processes with pre-defined rates can be found in the top row of Fig. 2. After each deposition or diffusion step, a cluster may take part in a growth process or be trapped. These processes, which are depicted in the bottom row of the figure, occur as instantaneous updates of the system and thus do not have specific rates. In Sec. II B, we explain how clusters and columns are “grown” in our simulations.

## B. Growth of nanocolumns

It is well known that the melting point of a bulk material decreases when the size of the material is reduced. As a consequence of this phenomenon, which is known as melting point depression, a small metal cluster typically shows a liquid-like behavior. When atoms or small clusters are added to such a cluster, it typically obtains a nearly spherical shape after a rapid equilibration process. However, if the temperature of the environment is fixed, a growing cluster undergoes a phase transition once it reaches a critical size. Such a solidification of a cluster leads to a modified growth mechanism:

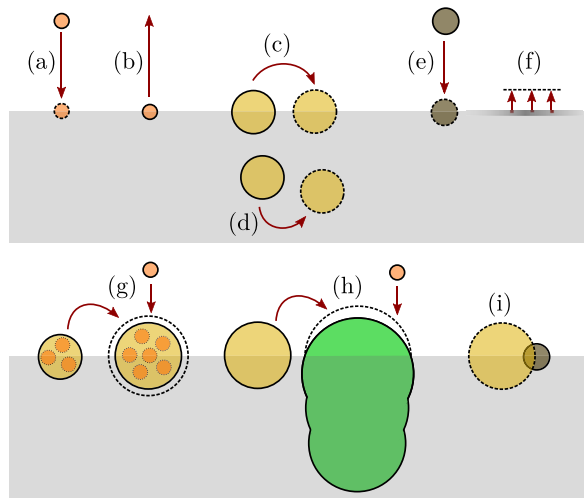


FIG. 2. Illustration of the simulation model (side view). The top row shows all processes that are controlled via rates: deposition (a) and desorption (b) of a monomer, surface diffusion (c), bulk diffusion (d), creation of a spherical defect in the polymer matrix (e), and a shift of the surface (f). The bottom row shows all possible updates that drive the formation of the metallic structure: spherical cluster growth by coalescence with another cluster or immediate addition of a deposited atom (g), columnar growth for sufficiently large clusters (h), and trapping of clusters that overlap with spherical defects (i).

since the mobility of the atoms in the cluster is strongly reduced, attached atoms stick to their initial positions. This implies that clusters grow into the preferred direction of the added particles.

In molecular dynamics simulations, the steady transition from a spherical to a rod-like growth can be simulated.<sup>29</sup> However, in KMC simulations, which are performed on much larger time scales, these observations have to be incorporated into an efficient model. We approach this problem by invoking two different growth models for the metallic structures. For the treatment of small liquid clusters, we use the liquid drop model, which has successfully been used in previous works.<sup>15,23</sup> The idea behind this model is that the cluster maintains a spherical shape, while the density of the individual atoms is conserved. If the cluster reaches a certain size, the growth mechanism is changed from spherical to columnar. The latter case is realized by a simple geometric solution: whenever a cluster is attached to an existing cluster or column, a sphere segment is added to its top. Similar to the liquid drop model, the size of these segments is chosen in a way that the density is conserved. While we restrict ourselves to a qualitative description of this process and show an illustration in Fig. 2, we refer to Ref. 15 for further mathematical details and simulation results. Nevertheless, we stress that the sphere segments are well suited to produce nanocolumns with very smooth boundaries, see Fig. 1, for example. So far, we only discussed the growth of the columns near the surface. However, if bulk diffusion is possible, clusters can also encounter the buried parts of a column. Due to the pressure of the surrounding polymer and the solid state of the column, we assume that a cluster just sticks to the column in such a case. This behavior breaks the radial symmetry of a column. Hence, if we want to compute an average thickness of the column, we assume that the volume of all

attached clusters is equally distributed around the columns. This is reasonable, because the number of attached clusters is usually quite high and the clusters have a nearly uniform radial distribution.

Since we distinguish between spherical clusters and columnar structures, our simulations allow us to separately track the number of clusters and columns. In Fig. 3, the  $\kappa$ -dependence of these numbers after the deposition process is illustrated for an exemplary parameter set. As one can see, by increasing  $\kappa$ , the system undergoes a slow transition from pure spherical cluster growth to columnar growth. For intermediate values of  $\kappa$ , both structures coexist. In our recent work,<sup>15</sup> we showed that the transition between both growth processes is usually connected with a sharp increase of the metallic volume filling factor. This can be explained by the fact that the columnar structures effectively prevent a large fraction of the monomers from evaporating since the columns provide an increased area of the surface that is covered with metal.

### III. RESULTS

We performed our simulations for surface fragments with the area  $300\text{ nm} \times 300\text{ nm}$ . The total heights of the grown composites were 100 nm. With these extensions, the total number of simulated metal atoms went up to  $5 \times 10^8$ , while the CPU times of each simulation run were always below  $\sim 10$  h.

Since the columns have spherical caps at their top and bottom parts, their final lengths may even be slightly larger than 100 nm. The diffusion constant of the metallic monomers was chosen to be  $D_s^1 = 1.7 \times 10^{-11} \text{ cm}^2/\text{s}$ . The critical cluster radius beyond which cluster growth transforms into columnar growth was set to  $r_c = 1.15 \text{ nm}$ , which corresponds to a cluster size of 500 atoms. We set this value by considering the results in Ref. 29, where the coalescence of two iron clusters with the sizes  $N = 250$  was only observed for temperatures greater than  $\sim 200$  K. Of course, since our simulations do not invoke temperature directly and, since there exist no data for the coalescence of Fe-Ni-Co clusters, the

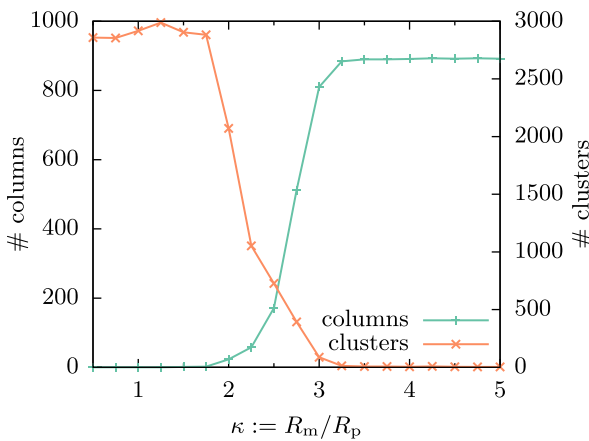


FIG. 3. Dependence of the number of nanocolumns and the number of (spherical) clusters on the ratio of metal and polymer deposition rates. The data correspond to the state of the nanocomposite after the deposition process. The simulations were performed with the evaporation rate  $R_e = 0.9 \nu_s^1$ .

value of the critical radius  $r_c$  is only a rough estimate. However, it is easy to modify the critical radius for a better fit to specific experimental conditions. The main effect of a modification of  $r_c$  is a shift of the value  $\kappa = R_m/R_p$  for which the column growth starts to dominate over the pure spherical growth: an increase of  $r_c$  will lead to an increase of the critical value of  $\kappa$ . Otherwise our results are expected to remain valid.

### A. Influence of pre-existing defects on the substrate

We start by analyzing the influence of surface defects that result from the initial preparation of the substrate, before we discuss the more complicated situation of defects that are being produced continuously during the deposition process (Sec. III B). This study is supposed to provide a basic understanding of how the defects affect the column growth processes. The defects are characterized by their areal number density  $\rho = N_{\text{defects}}/A$ , where  $N_{\text{defects}}$  is the total number of defects and  $A$  is the area of the substrate. We start the discussion with the case of defects that are distributed on a hexagonal lattice in Sec. III A 1. Although such a configuration is not expected in many applications, we use it to demonstrate an idealized behavior, where each defect has the same probability to be the source of a nanocolumn. As a next step, in Sec. III A 2, we show how these results are affected by a randomization of the defect structure.

#### 1. Hexagonal defect pattern

If one wants to produce a regular pattern of nanocolumns, it is important that the nucleation of clusters happens at preferred sites. While this requirement may demand a big experimental effort, it can easily be realized in the simulations by distributing the defects in the desired way. For this study, we chose a hexagonal set-up of the defects. In Figs. 4(a)–4(c), the  $\kappa$ -dependent column properties are shown for different densities  $\rho$ . The most obvious influence of  $\rho$  can be seen in the total number of nanocolumns Fig. 4(a). For the density  $\rho = 1 \times 10^{-2} \text{ nm}^{-2}$ , the dependence on the ratio  $\kappa$  is similar to the one that we observed in Ref. 15: for an intermediate value  $\kappa \approx 2.5$ , the column growth sets in and there is a steep increase of the number of columns, before the value saturates, for larger  $\kappa$ . Such a saturation occurs when each defect is the origin of a column. In this case, the number of columns is given by the value  $\rho A$ , which is also indicated by a dashed line. For the increased density,  $\rho = 3 \times 10^{-2} \text{ nm}^{-2}$ , a similar behavior is observed. However, the growth sets in for higher values of  $\kappa$  and the maximum number of columns is larger. This can be explained by the increased competition between the numerous nucleation sites. Only if enough metal atoms are deposited, all (or most of) the initially formed clusters can turn into columns. If  $\rho$  is further increased to  $5 \times 10^{-2} \text{ nm}^{-2}$ , this effect becomes so important that it leads to a strong suppression of the column growth. In the opposite case of very low defect densities, e.g.,  $1 \times 10^{-4} \text{ nm}^{-2}$ , the number of columns is also relatively small. However, in this case, the reason is the strongly increased number of metal atoms that re-evaporate from the surface due to the lack of preferred nucleation sites. Furthermore, the number of

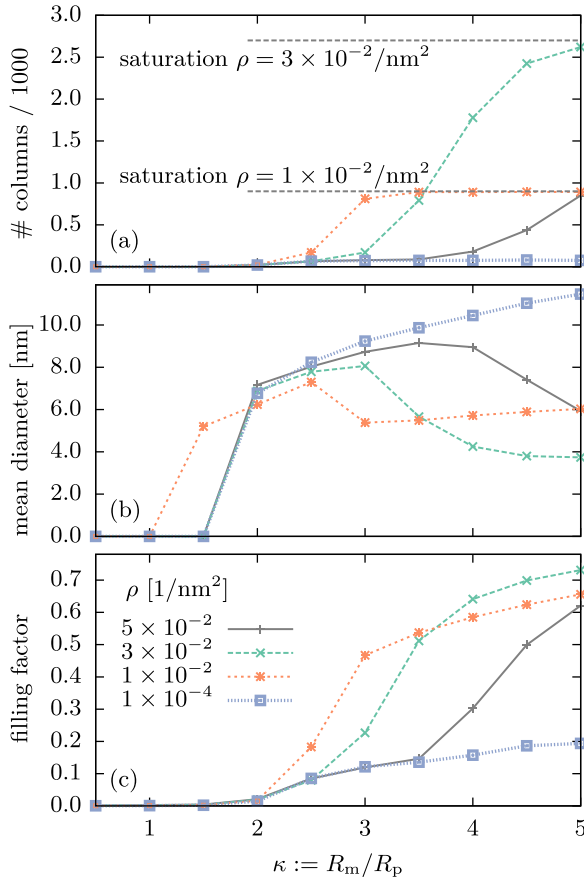


FIG. 4. Simulation results for different number densities  $\rho$  of defects on the substrate. The defects were distributed on a hexagonal lattice. The evaporation rate for the results is  $R_e = 0.9 \nu_s^1$ .

columns is even higher than the number of defects, which is possible if columns are formed at arbitrary positions between the initially created defect sites.

The thicknesses of the columns, Fig. 4(b), can be understood as the result of an interplay between two opposing trends. On the one hand, by increasing  $\kappa$ , more metal atoms are provided that might eventually increase the thickness of an existing column. On the other hand, the total number of columns may grow, which leads to increased competition effects and, thus, thinner columns. Especially for  $\rho = 1 \times 10^{-2} \text{ nm}^{-2}$  it is obvious how this behavior results in a local maximum of the mean diameter, around  $\kappa = 2.5$ , and a slow monotonic increase of the value for larger  $\kappa$  in the saturated regime. With the exception of  $\rho = 1 \times 10^{-4} \text{ nm}^{-2}$ , where the number of columns is very small, a similar behavior is observed for all other defect densities.

Since most of the metallic volume in the nanocomposite is contained in the columnar structures, it is clear that the metallic filling factor, Fig. 4(c), is connected to both, the number of columns and the column thickness. For instance, the transition from spherical to columnar growth is reflected by the sharp increase of the filling factor. At the same time, if the number of columns reaches saturation, the growing thickness of the columns still leads to a slight increase of the filling factor. This behavior is most obvious for the density  $\rho = 1 \times 10^{-2} \text{ nm}^{-2}$ . A further indicator of the relationship between all of the three quantities is the fact that there exist

$\kappa$ -values, for which the curves of all quantities intersect, although they correspond to different defect densities. For instance, these intersections can be observed for the densities  $\rho = 1 \times 10^{-2} \text{ nm}^{-2}$  and  $5 \times 10^{-2} \text{ nm}^{-2}$ , at  $\kappa = 3.5$  and 5.

Completing the discussion of the geometric properties of the columns, we refer to the distribution of column lengths shown in Fig. 5. As expected, in most cases, the columns extend from the bottom to the top of the nanocomposite. However, one can see that a sufficiently high density of defects is required to obtain a distribution with a sharp peak around 100 nm. For the small value  $\rho = 1 \times 10^{-4} \text{ nm}^{-2}$ , the uniformity of the composite is disturbed by the occurrence of smaller columns.

The above results demonstrate how the simulations allow us to define parameter ranges that are best suited to produce uniform nanocolumns. The strong influence of the surface defects shows that the properties of the final composite are already set at the early stage of the deposition process. Furthermore, we remark that the nanocolumns noticeably increase their thickness shortly before they attain a rather constant diameter. A similar behavior, which is also revealed in the rendered image in Fig. 1, was observed in Ref. 30.

## 2. Random defect distribution

For the modeling of many realistic experimental scenarios, it is more appropriate to assign each defect a random position on the substrate. In comparison with the results shown in Fig. 4, the qualitative behavior is the same and there is even a good quantitative agreement for many parameter settings. In Fig. 6(a), one can see that the randomization mainly leads to a reduced total number of columns for some values of the density  $\rho$ . While there is nearly perfect agreement between the data for the small density  $\rho = 1 \times 10^{-4} \text{ nm}^{-2}$ , the saturated number of columns is slightly reduced for  $\rho = 1 \times 10^{-2} \text{ nm}^{-2}$  and  $3 \times 10^{-2} \text{ nm}^{-2}$ . For very high defect densities, e.g.,  $\rho = 5 \times 10^{-2} \text{ nm}^{-2}$ , there is a noticeable quantitative deviation from the results in the case of a hexagonal distribution. However, one can still observe the same tendency of a suppressed column growth, which is due to the highly increased competition between nucleation sites. The mean diameters of the columns and the filling factors, which

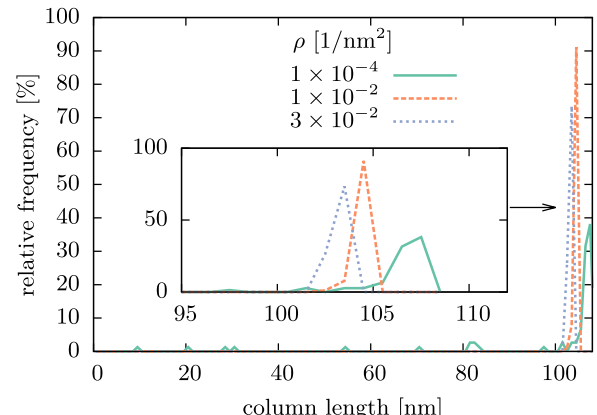


FIG. 5. Distribution of column lengths for  $\kappa = 5.0$ ,  $R_e = 0.9 \nu_s^1$  and different number densities  $\rho$  of surface defects.

are shown in Figs. 6(b) and 6(c), do not need to be discussed in detail, because their relation to the number of columns is the same as has been described in Sec. III A 1, cf. Fig. 4.

The main reason for the reduced number of columns compared to the hexagonal lattice is that two or more defects have a finite probability to be so close to each other that they effectively act as a joint origin for just a single column. The occurrence of such a behavior grows with the defect density. In the case of a hexagonal defect pattern and moderate densities  $\rho$ , we showed that one can accurately determine the saturated number of columns by  $N_{\text{columns}} = \rho A$ . If the defects are distributed randomly, it is possible to make a similar estimation,  $N_{\text{columns}} = \rho_{\text{eff}} A$ , introducing the effective number density of defects

$$\rho_{\text{eff}} = k(\rho)\rho. \quad (5)$$

The factor  $(1 - k)$  determines the fraction of defects that are very close to other existing defects and hence are not expected to be the source of an additional column.

Aiming at the prediction of  $N_{\text{columns}}$  for random defect configurations, we performed a separate investigation to determine the  $\rho$ -dependence of  $k$ . For that purpose, we applied a simple Monte Carlo scheme to find the minimum number of spheres with the critical radius  $r_c$  that are required to cover all defects on a two-dimensional plane. While the defects are represented by randomly distributed spheres with

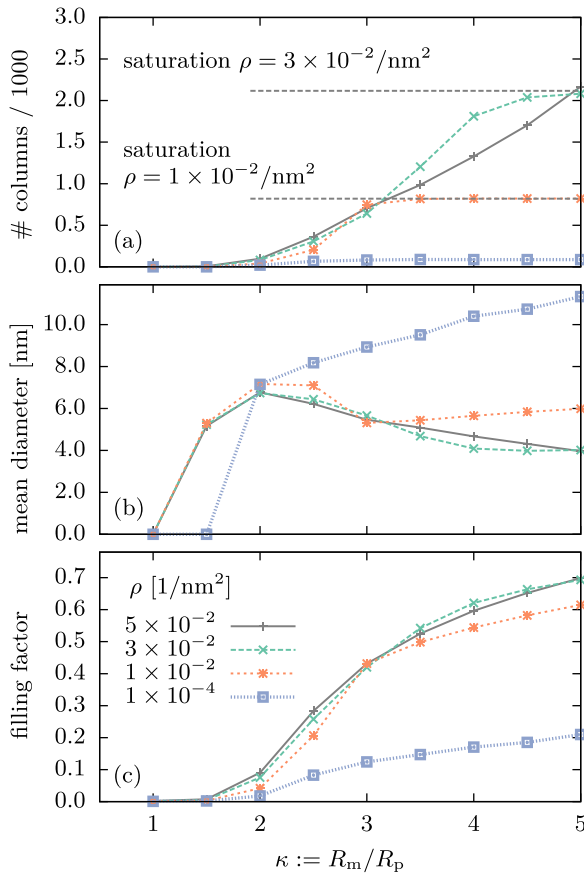


FIG. 6. Simulation results for different number densities  $\rho$  of randomly distributed defects on the substrate. The evaporation rate for the results is  $R_e = 0.9 \nu_s^1$ .

the radius  $r_{\text{defect}}$ , the larger spheres are intended to represent the clusters, before their growth is changed from spherical to columnar. The most accurate predictions could be made by defining a defect as being covered if the distance between its center and the center of the column sphere is less than  $r_c + 0.5 r_{\text{defect}}$ . This choice involves a certain degree of freedom, but we checked that the resulting values of  $k$  are only weakly affected by different definitions. For clarity, the idea of the covering is illustrated in Fig. 7(a) for a selected random configuration of defects with the number density  $\rho = 3 \times 10^{-2} \text{ nm}^{-2}$ . Averaging over many different configurations at different densities, we obtained the  $\rho$ -dependent values of  $k$  that are shown in Fig. 7(b). As expected,  $k$  is quite close to 1 for small densities, i.e., most defects are far away from each other, and it is very likely that each defect results in the growth of a nanocolumn. In addition to this, one can again expect that some columns also grow at arbitrary positions between the defects. For densities up to the value  $\rho = 1 \times 10^{-2} \text{ nm}^{-2}$ , which we use for the results in Secs. III B and III C,  $k$  remains greater than 0.9, i.e., the explicit type of the defect distribution has only very a weak influence on the numerical data. For high densities, where almost all defects are closer than the critical radius,  $k$  approaches zero. Although this limit is not of practical relevance, we stress that in the transition from moderate to very high densities, starting around  $\rho = 3.0 \times 10^{-2} \text{ nm}^{-2}$ , the explicit distribution of the defects clearly affects the quantitative results. Being able to make predictions for the saturated number of columns with these results, we indicate the corresponding values by the dashed lines in Fig. 6(a). Apparently, for the medium densities  $\rho = 1 \times 10^{-2} \text{ nm}^{-2}$  and  $3 \times 10^{-2} \text{ nm}^{-2}$ , the predictions are very accurate. However, the predictions cannot hold for higher densities, because the number of columns does not reach a saturated value anymore. For low densities, it is not possible either, because the ratio between the number of columns and the number of defects is even greater than one.

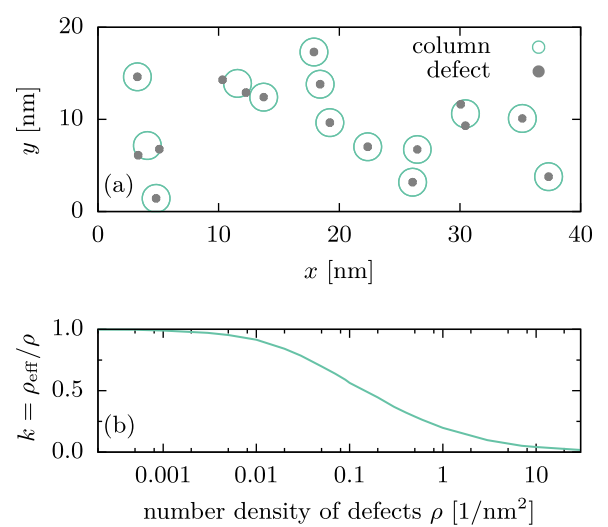


FIG. 7. (a) Exemplary distribution of defects and column origins on the substrate for the defect density  $\rho = 3.0 \times 10^{-2} \text{ nm}^{-2}$ . (b) Density-dependent values of the factor  $k$ , which is used in Eq. (5) to calculate the effective density of defects.

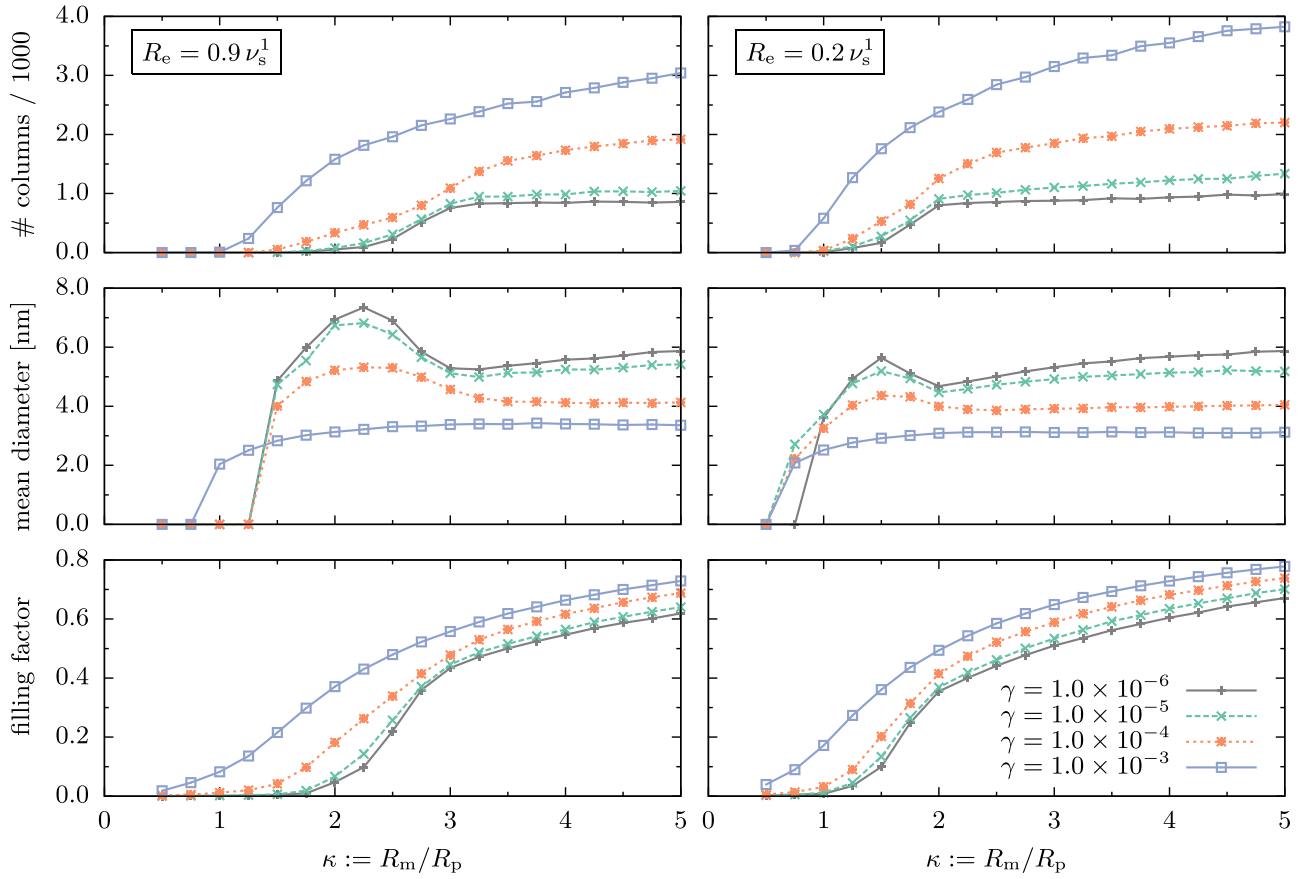


FIG. 8. Influence of the ratio  $\gamma = R_{\text{defect}}/R_m$  on the column properties for two different evaporation rates  $R_e$ . The initial density of randomly distributed defects was  $\rho = 1 \times 10^{-2} \text{ nm}^{-2}$ .

## B. Random defect creation during deposition

In the following, we investigate the more complex situation, where defect sites may be created at random times during the deposition process. For these simulations we chose a random initial distribution of defects and fixed the density to  $\rho = 1 \times 10^{-2} \text{ nm}^{-2}$ . In Fig. 8, the  $\kappa$ -dependent column properties are shown for different values of the critical parameter  $\gamma = R_{\text{defect}}/R_m$  and the two different evaporation rates  $R_e = 0.9 \nu_s^1$  (left) and  $R_e = 0.2 \nu_s^1$  (right). For both evaporation rates and  $\gamma$ -values up to  $1 \times 10^{-5}$ , the influence of the defects on the total number of columns, the diameter of the columns and the metallic filling factor is very weak. Hence, the column properties are similar to those shown in Fig. 4. However, between  $\gamma = 1 \times 10^{-4}$  and  $1 \times 10^{-3}$ , the metallic structure of the composites changes drastically. The high number of defects strongly arrests the diffusion and the evaporation of monomers. Consequently, the number of preferred nucleation sites is highly increased. These sites trap many clusters, some of which turn into columnar structures. This can be seen in the total number of columns, which is plotted in the top row of the figure. For large  $\gamma$  values, the number of columns is strongly increased, and the typical saturation tends to vanish. Furthermore, the column growth already sets in for lower ratios  $\kappa$ . Similarly to the previous observations in Sec. III A, the increased number of columns is connected to a reduced column thickness (middle row) and an increase of the filling factor (bottom row). For all investigated

evaporation rates, the defects have very similar consequences. However, if the evaporation rate is decreased, the reduced probability for an atom to be re-emitted shifts the features of the column properties to lower values of  $\kappa$ .

In contrast to the simulation without random defects, a consequence of the additional trapping sites is that the origins of the columns are observed at arbitrary heights in the polymer matrix. This is demonstrated in Fig. 9, which shows the distribution of column origins in vertical direction for

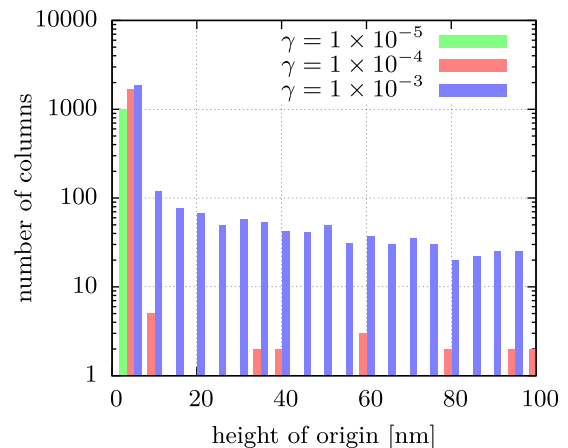


FIG. 9. Influence of the ratio  $\gamma = R_{\text{defect}}/R_m$  on the origin of the columns in vertical direction. The parameters are  $\kappa = 4$  and  $R_e = 0.9 \nu_s^1$ . For each  $\gamma$ , the bin widths are 5 nm.

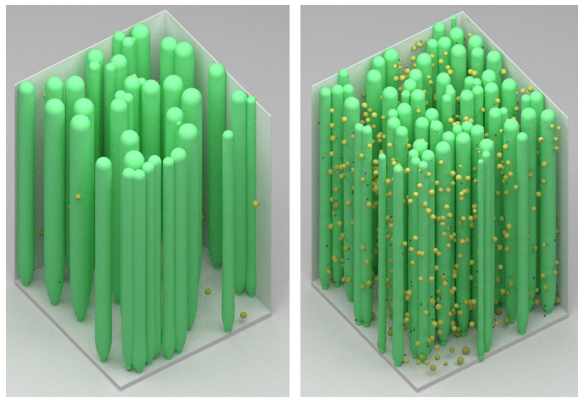


FIG. 10. Visualization of the simulation results for  $\gamma = 1 \times 10^{-6}$  (left) and  $\gamma = 1 \times 10^{-4}$  (right). In both images, the areas of the substrate have the same size  $60 \times 60 \text{ nm}^2$ . The objects with the colors green, yellow, and black correspond to columns, spherical clusters, and defects, respectively. The polymer is not shown in these pictures, but it is assumed to fill the space between the columns and clusters.

different values of  $\gamma$ . Although the origins of most columns remain at the bottom area in the polymer for all  $\gamma$ , there is a highly increased chance for columns to be formed at higher positions in the regime  $\gamma \geq 1 \times 10^{-3}$ .

In addition to the numerical data, in Fig. 10, we provide rendered images of the simulation results for different  $\gamma$ . For the small value  $\gamma = 1 \times 10^{-6}$ , the resulting columnar structure is almost exclusively induced by the initial defects on the substrate. The additional defects during the deposition process mainly result in the occurrence of some clusters at arbitrary positions in the polymer matrix. For the higher value,  $\gamma = 1 \times 10^{-4}$ , not only the number of additional clusters but also the number of columns is highly increased. Nevertheless, according to the results in Fig. 9, most columns still have their origins at the bottom of the composite.

### C. Influence of bulk diffusion

In order to understand the trends arising from bulk diffusion, we varied the free parameter  $r_{s/b}$  in the range from extremely small values, on the order of 1, to more realistic values, between 40 and 60.<sup>21,24</sup> The resulting column properties for selected values of the parameter  $\gamma$  are shown in Fig. 11. The figure only shows results for up to  $r_{s/b} = 20$ , because the deviations from the limit  $r_{s/b} \rightarrow \infty$  are already unnoticeable in this regime. Even for the ratio  $r_{s/b} = 5$ , the bulk diffusion has only a minor influence. However, especially by considering the very small value  $r_{s/b} = 1$ , the physical trends become clear.

Starting the discussion for a small number of defects,  $\gamma = 1 \times 10^{-6}$ , (left column of the figure), one observes a behavior that is similar to that shown in Fig. 4 for medium defect densities  $\rho$ . The number of columns exhibits a sudden increase to a saturated value if  $\kappa$  is raised. This holds for all  $r_{s/b}$ , but by lowering  $r_{s/b}$ , the column growth is already observed for smaller values of  $\kappa$ . This can be explained by the increased mobility of buried particles leading to an increased number of cluster and column growth events. Furthermore, one again observes the previously mentioned local maxima of the mean column width. For the very small

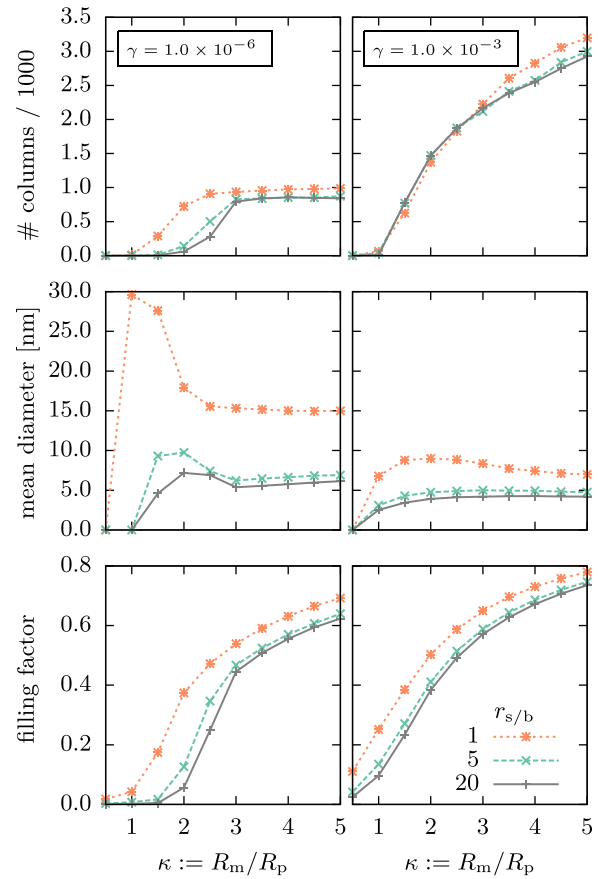


FIG. 11. Column properties for simulations with different bulk diffusion constants. The parameter  $r_{s/b}$  labels the ratio of the surface and the bulk diffusion constants for monomers, see Eqs. (3) and (4). The results are shown for both small (left) and large (right) rates for the creation of defects,  $R_{\text{defect}} = \gamma R_m$ . The data were produced with the evaporation rate  $R_e = 0.9 \nu_s^1$  and the initial density of randomly distributed defects  $\rho = 1 \times 10^{-2} \text{ nm}^{-2}$ .

value  $r_{s/b} = 1$ , the maximum is especially pronounced. Beyond the maxima, i.e., for larger values of  $\kappa$ , the width of the columns shrinks if the number of columns grows. Considering the filling factor, one observes the expected steep increase that is directly related to the growth of columns. While this is the case for all investigated values of  $r_{s/b}$ , a decrease of  $r_{s/b}$  generally leads to higher filling factors, because the growing importance of the bulk diffusion process causes a decreased probability of re-emission of deposited monomers. In addition to these specific details, we remark that the influence of bulk diffusion is generally reduced when  $\kappa$  is increased. This can be explained by the fact that the nanocolumns—which are likely to exist for large  $\kappa$ —have a high chance to absorb the deposited particles and, hence, suppress both the surface and the bulk diffusion processes.

If the number of defects is increased by raising the parameter  $\gamma$ , the bulk diffusion becomes less important, due to an increased number of trapping events. This is revealed by the results for the high value,  $\gamma = 1 \times 10^{-3}$ , that are shown in the right column of Fig. 11. For  $r_{s/b}$ -values larger than 5, no significant difference to the behavior without bulk diffusion is observed, see also the previous results in Fig. 8 for comparison. Deviations only evolve by lowering  $r_{s/b}$  down to

the value 1. In this case, the most obvious trend is the increase of the metallic filling factor for all  $\kappa$ . However, this is not necessarily due to an increased number of columns. For instance, it is noticeable that the total number of columns is slightly reduced, for  $\kappa \leq 2.5$ , and increased, for larger values of  $\kappa$ . This means that—at least for intermediate  $\kappa$ —there exist many additional clusters besides the columns.

Since the mentioned effects are relatively weak for realistic values of  $r_{s/b}$ , it is justified to ignore the bulk diffusion in the relevant cases. The reason for this is the fact that most monomers either take part in a growth process on the surface or they are re-emitted. However, for very low evaporation rates, it is more likely that a cluster is buried in the bulk, and thus the bulk diffusion is expected to gain a greater importance, in this case. Although the temperature is not included directly in the simulations, we expect that even upon strong variation of the temperature, the diffusion on the surface will remain much faster than the bulk diffusion. Without bulk diffusion the greatest speedups of the CPU time, which are typically around a factor of 3 for  $R_e = 0.2 \nu_s^1$ , are achieved for the smallest values of  $\gamma$  and  $\kappa$ .

#### IV. CONCLUSIONS

In this work, we showed, by means of kinetic Monte Carlo simulations, how the recently investigated formation of nanocolumns<sup>14,15</sup> in a metal-polymer nanocomposite is affected if the metal atoms are produced in a sputtering instead of an evaporation source. Our main goal was to answer the question whether the column growth is possible at all in such a plasma environment. An important additional effect of the sputter deposition method is the frequent impingement of ions on the substrate. These ions generate defects on the polymer surface, which have the tendency to trap metal clusters. Since this effect limits the diffusion of metal particles, it is *a priori* an open question whether the self-organized process of the column growth will be inhibited or completely prevented. According to our simulation results, we predict that the ion defects in a plasma environment do not prevent but even enhance the column growth. The parameters given in the present work should allow for an experimental verification of this result.

To capture the main plasma environment conditions, we extended our previous simulation model by adding a process which generates spherical defects at random positions on the surface. Acting as instantaneous traps for metal clusters of all sizes, the defects prevent the movement and evaporation of all clusters that come sufficiently close. This trapping leads to preferred growth of clusters and columns near a defect. For all investigated values of  $\gamma$ , which controls the number of created defects, the number of columns is increased. At the same time, the mean width of the columns is reduced, due to competition effects. The most noticeable influence of the defects sets in if  $\gamma$  is of the order  $1 \times 10^{-4}$ . In this regime, many additional columns start to grow, not only at the bottom but also at the arbitrary vertical positions in the bulk. We demonstrated that these results are only weakly affected if one neglects bulk diffusion of the metal clusters.

The complexity of the investigated systems forced us to base our model on several strong simplifications. Although the predictive power of these types of simulation has already been demonstrated,<sup>15,23</sup> it is clear that for a quantitatively accurate simulation of column growth in a plasma-based experiment, some additional properties and processes will have to be taken into account. In particular, this comprises the charging of particles and clusters which will be analyzed in the future. Furthermore, we neglected the exact geometric details of the defects, e.g., their specific shapes and penetration depths. However, we expect that our model of a defect yields an accurate statistical behavior, which could be easily improved by an adjustment of the defect radii or the introduction of a finite trapping probability smaller than one.

#### ACKNOWLEDGMENTS

This work was supported by the Deutsche Forschungsgemeinschaft via SFB-TR 24 (projects A5 and B13). N.K. acknowledges support from the German Academic Exchange Service via the RISE program. We thank the developers of Blender<sup>31</sup> for providing a useful tool for the visualization of the simulation results.

- <sup>1</sup>A. Pomogailo and V. Kestelman, *Metallopolymer Nanocomposites*, Materials science (Springer, 2005).
- <sup>2</sup>T. A. Fulton and G. J. Dolan, *Phys. Rev. Lett.* **59**, 109 (1987).
- <sup>3</sup>H. Graf, J. Vancea, and H. Hoffmann, *Appl. Phys. Lett.* **80**, 1264 (2002).
- <sup>4</sup>H. Takele, S. Jebril, T. Strunskus, V. Zaporjchenko, R. Adelung, and F. Faupel, *Appl. Phys. A* **92**, 345 (2008).
- <sup>5</sup>M. Karttunen, P. Ruuskanen, V. Pitkänen, and W. M. Albers, *J. Electron. Mater.* **37**, 951 (2008).
- <sup>6</sup>A. Biswas, O. Aktas, J. Kanzow, U. Saeed, T. Strunskus, V. Zaporjchenko, and F. Faupel, *Mater. Lett.* **58**, 1530 (2004).
- <sup>7</sup>A. Biswas, O. Aktas, U. Schürmann, U. Saeed, V. Zaporjchenko, F. Faupel, and T. Strunskus, *Appl. Phys. Lett.* **84**, 2655 (2004).
- <sup>8</sup>A. Emamifar, *Applications of Antimicrobial Polymer Nanocomposites in Food Packaging*, edited by A. Haschim, Advances in Nanocomposite Technology (InTech, 2011).
- <sup>9</sup>F.-R. F. Fan and A. J. Bard, *J. Phys. Chem. B* **106**, 279 (2002).
- <sup>10</sup>F. Faupel, V. Zaporjchenko, H. Greve, U. Schürmann, V. S. K. Chakravadhanula, C. Hanisch, A. Kulkarni, A. Gerber, E. Quandt, and R. Podschun, *Contrib. Plasma Phys.* **47**, 537 (2007).
- <sup>11</sup>G. V. Ramesh, S. Porel, and T. P. Radhakrishnan, *Chem. Soc. Rev.* **38**, 2646 (2009).
- <sup>12</sup>Q. Wang and L. Zhu, *ACS Symposium Series 1034, Functional Polymer Nanocomposites for Energy Storage and Conversion* (American Chemical Society, 2010).
- <sup>13</sup>*Complex Plasmas: Scientific Challenges and Technological Opportunities*, edited by M. Bonitz, J. Lopez, K. Becker, and H. Thomsen, Springer Series on Atomic, Optical, and Plasma Physics (Springer Verlag, 2014), Vol. 82.
- <sup>14</sup>H. Greve, A. Biswas, U. Schürmann, V. Zaporjchenko, and F. Faupel, *Appl. Phys. Lett.* **88**, 123103 (2006).
- <sup>15</sup>L. Rosenthal, H. Greve, V. Zaporjchenko, T. Strunskus, F. Faupel, and M. Bonitz, *J. Appl. Phys.* **114**, 044305 (2013).
- <sup>16</sup>H. Biederman, in *Proceedings of the Fifth International Symposium on Sputtering and Plasma Processes* [Vacuum **59**, 594 (2000)].
- <sup>17</sup>D. M. Mattox, *J. Vac. Sci. Technol. A* **7**, 1105 (1989).
- <sup>18</sup>J. Ziegler, J. Biersack, and M. Ziegler, *SRIM, the Stopping and Range of Ions in Matter* (SRIM Company, 2008).
- <sup>19</sup>M. Ziegler, J. Kröger, R. Berndt, A. Filinov, and M. Bonitz, *Phys. Rev. B* **78**, 245427 (2008).
- <sup>20</sup>A. Jansen, *An Introduction to Kinetic Monte Carlo Simulations of Surface Reactions*, Lecture notes in physics (Springer-Verlag, 2012).
- <sup>21</sup>L. Rosenthal, T. Strunskus, F. Faupel, J. W. Abraham, and M. Bonitz, *Kinetic Monte Carlo Simulations of Cluster Growth and Diffusion in Metal-Polymer Nanocomposites*, Chapter in Ref. 13.

- <sup>22</sup>M. Bonitz, L. Rosenthal, K. Fujioka, V. Zaporotchenko, F. Faupel, and H. Kersten, *Contrib. Plasma Phys.* **52**, 890 (2012).
- <sup>23</sup>L. Rosenthal, A. Filinov, M. Bonitz, V. Zaporotchenko, and F. Faupel, *Contrib. Plasma Phys.* **51**, 971 (2011).
- <sup>24</sup>L. Rosenthal, "Kinetic Monte Carlo simulations of metal-polymer nano-composite formation," Ph.D. thesis (University of Kiel, 2013).
- <sup>25</sup>A. Thran, M. Kiene, V. Zaporotchenko, and F. Faupel, *Phys. Rev. Lett.* **82**, 1903 (1999).
- <sup>26</sup>F. Faupel, R. Willecke, and A. Thran, *Mater. Sci. Eng. R* **22**, 1 (1998).
- <sup>27</sup>D. Gupta, *Diffusion Processes in Advanced Technological Materials* (William Andrew Pub., 2010).
- <sup>28</sup>M. H. Cohen and D. Turnbull, *J. Chem. Phys.* **31**, 1164 (1959).
- <sup>29</sup>F. Ding, A. Rosén, and K. Bolton, *Phys. Rev. B* **70**, 075416 (2004).
- <sup>30</sup>E. Main, T. Karabacak, and T. M. Lu, *J. Appl. Phys.* **95**, 4346 (2004).
- <sup>31</sup>Blender Online Community, *Blender—A 3D Modelling and Rendering Package* (Blender Foundation, Blender Institute, Amsterdam).